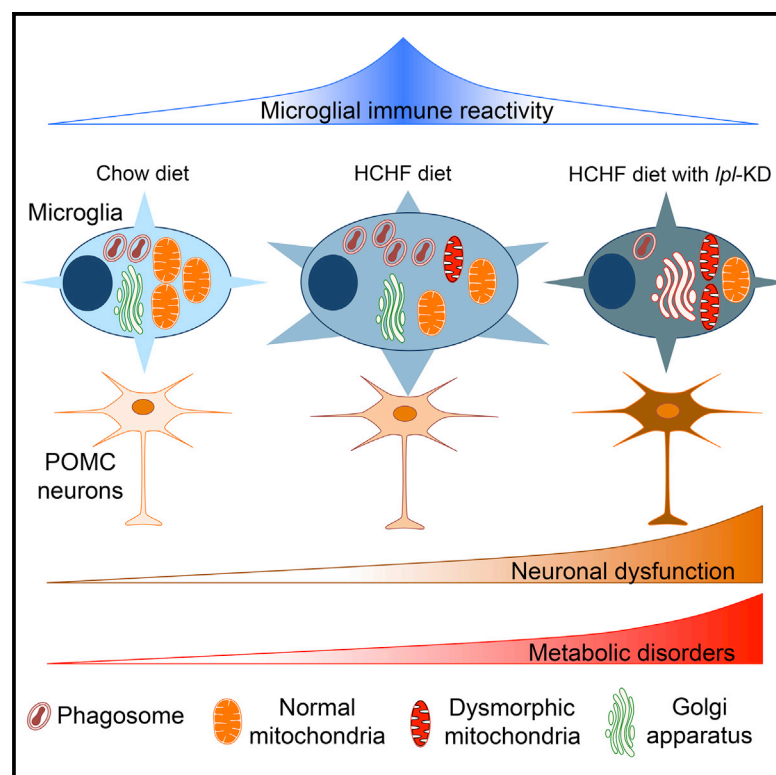


Cell Reports

Lipoprotein Lipase Maintains Microglial Innate Immunity in Obesity

Graphical Abstract



Authors

Yuanqing Gao, Andrés Vidal-Itriago, Martin J. Kalsbeek, ..., Robert H. Eckel, Susanna M. Hofmann, Chun-Xia Yi

Correspondence

c.yi@amc.uva.nl

In Brief

Microglia are brain macrophages responsible for immune defense. LPL is a key enzyme gating lipid uptake by microglia. Gao et al. show that loss of *Lpl* in microglia results in downregulation of immune reactivity. Mice with knockdown of the *Lpl* gene in microglia are more vulnerable to diet-induced metabolic syndrome.

Highlights

- High-carbohydrate high-fat diet stimulates microglial *Lpl* gene expression
- Mitochondrial fuel utilization switches to glutamine in microglia lacking LPL
- Microglial immune reactivity is impaired in microglia lacking LPL
- POMC neuronal loss is accelerated when microglia lack LPL



Lipoprotein Lipase Maintains Microglial Innate Immunity in Obesity

Yuanqing Gao,¹ Andrés Vidal-Itriago,¹ Martin J. Kalsbeek,¹ Clarita Layritz,² Cristina García-Cáceres,² Robby Zachariah Tom,³ Thomas O. Eichmann,⁴ Frédéric M. Vaz,⁵ Riekelt H. Houtkooper,⁵ Nicole van der Wel,⁶ Arthur J. Verhoeven,⁷ Jie Yan,⁸ Andries Kalsbeek,^{1,9} Robert H. Eckel,¹⁰ Susanna M. Hofmann,³ and Chun-Xia Yi^{1,11,*}

¹Department of Endocrinology and Metabolism, Academic Medical Center, University of Amsterdam, the Netherlands

²Helmholtz Diabetes Center & German Center for Diabetes Research, Helmholtz Zentrum München & Division of Metabolic Diseases, Technische Universität München, Munich, Germany

³Institute for Diabetes and Regeneration Research & Helmholtz Diabetes Center, Helmholtz Zentrum München, Medizinische Klinik und Poliklinik IV, Klinikum der LMU, Munich, Germany

⁴Institute of Molecular Biosciences, University of Graz, Austria

⁵Laboratory Genetic Metabolic Diseases, Academic Medical Center, University of Amsterdam, the Netherlands

⁶Cellular Imaging Core Facility, Academic Medical Center, University of Amsterdam, the Netherlands

⁷Department of Medical Biochemistry, Academic Medical Centre, University of Amsterdam, the Netherlands

⁸Department of Forensic Science, School of Basic Medical Science, Central South University, Changsha, Hunan, China

⁹Hypothalamic Integration Mechanisms, Netherlands Institute for Neuroscience, Amsterdam, the Netherlands

¹⁰Division of Endocrinology, Metabolism and Diabetes, University of Colorado School of Medicine, Aurora, CO, USA

¹¹Lead Contact

*Correspondence: c.yi@amc.uva.nl

<http://dx.doi.org/10.1016/j.celrep.2017.09.008>

SUMMARY

Consumption of a hypercaloric diet upregulates microglial innate immune reactivity along with a higher expression of lipoprotein lipase (*Lpl*) within the reactive microglia in the mouse brain. Here, we show that knockdown of the *Lpl* gene specifically in microglia resulted in deficient microglial uptake of lipid, mitochondrial fuel utilization shifting to glutamine, and significantly decreased immune reactivity. Mice with knockdown of the *Lpl* gene in microglia gained more body weight than control mice on a high-carbohydrate high-fat (HCHF) diet. In these mice, microglial reactivity was significantly decreased in the mediobasal hypothalamus, accompanied by downregulation of phagocytic capacity and increased mitochondrial dysmorphologies. Furthermore, HCHF-diet-induced POMC neuronal loss was accelerated. These results show that LPL-governed microglial immunometabolism is essential to maintain microglial function upon exposure to an HCHF diet. In a hypercaloric environment, lack of such an adaptive immunometabolic response has detrimental effects on CNS regulation of energy metabolism.

INTRODUCTION

Microglia are brain macrophages responsible for innate immune reactivity, which is essential for maintaining a local microenvironment optimal for neuronal survival and functioning (Kettenmann et al., 2011; Li et al., 2012; Prinz and Priller, 2014). In high-carbohydrate high-fat (HCHF)-diet-induced obese mice,

microglial reactivity in the hypothalamus increases (Gao et al., 2014; Thaler et al., 2012). Intracellular metabolism is closely related with the function of immune cells (O'Neill et al., 2016). Activated immune cells such as macrophages and T cells have high metabolic demands (Newsholme et al., 1986; Oren et al., 1963) and thus require a higher fuel influx. One of the key enzymes involved in cellular fuel uptake is lipoprotein lipase (LPL), the enzyme that delivers lipids by catalyzing triglyceride (TG)-rich lipoproteins (Wang and Eckel, 2009). On a high-fat atherogenic diet, LPL in mouse macrophages is important for promoting foam cell formation through the degradation and internalization of lipoproteins (Babaev et al., 1999). Among the different types of brain cells, microglia show the highest level of *Lpl* mRNA expression (Zhang et al., 2014; Zhang et al., 2016). When we compared isolated hypothalamic microglia from standard chow-diet-fed lean mice and HCHF-diet-induced obesity (DIO) mice, we detected a significant increase in *Lpl* gene expression in DIO mice, indicating that LPL might be involved in the activation of hypothalamic microglia in animals on an HCHF diet. We therefore generated ex vivo and in vivo models with microglia-specific knockdown of the *Lpl* gene and studied microglial immunometabolism and hypothalamic neural responses to hypercaloric challenges.

RESULTS

Lpl Gene Expression Is Highest in Hypothalamic Microglia

In primary cultured hypothalamic neurons, astrocytes, and microglia, we observed the highest *Lpl* mRNA level in microglia (Figure 1A). In isolated hypothalamic microglia from mice that had been on an HCHF diet for 1 day, 3 days, 7 days, 28 days, or 10 weeks, microglial *Lpl* gene expression increased after 3 days on the HCHF diet compared with mice on a chow diet, except for a transient decline on day 7 (Figure 1B). These data

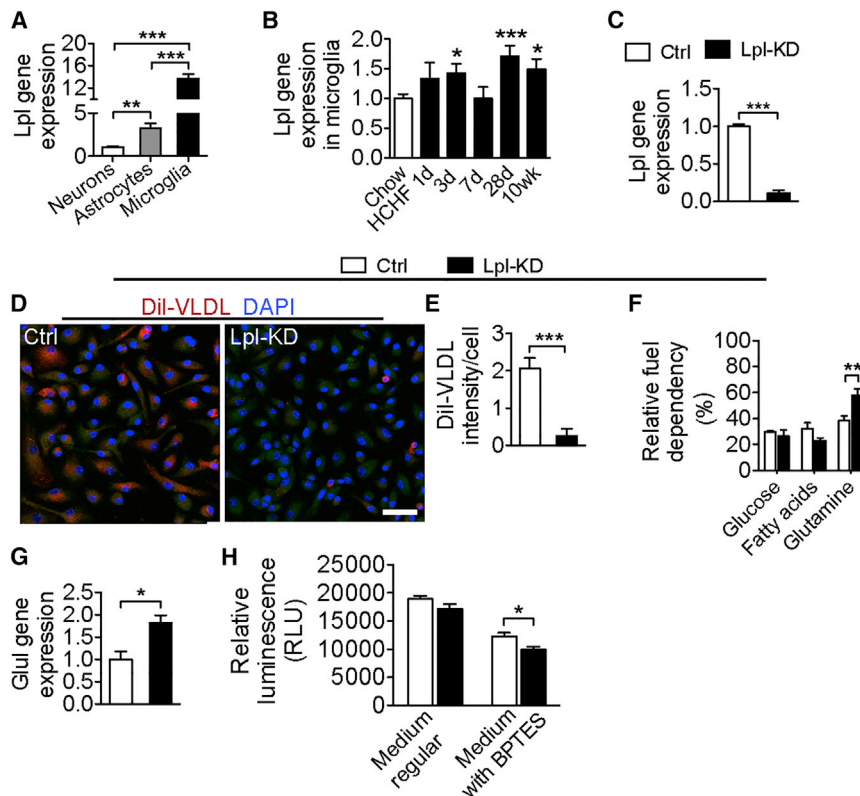


Figure 1. LPL in Microglia Governs Microglial Immunometabolism

(A) *Lpl* mRNA levels in hypothalamic primary neurons (n = 5), astrocytes (n = 4), and microglia (n = 3).
(B) The *Lpl* mRNA level is higher in hypothalamic microglia isolated from mice on an HCHF diet for 3 days, 28 days, and 10 weeks (n = 4–11) than from chow-diet-fed mice (n = 7).
(C) The *Lpl* mRNA level is significantly down-regulated in *Lpl*-KD microglia in primary cultures with 5 days of 4-hydroxytamoxifen treatment; n = 7 per group.
(D) Dil-VLDL uptake in primary microglia.
(E) Dil-VLDL uptake is significantly blocked in primary *Lpl*-KD microglia, n = 6 per group.
(F) Relative fuel dependency in Ctrl microglia (n = 6–11) and *Lpl*-KD microglia (n = 7–11).
(G) The glutamine synthetase (*Glut*) mRNA level is significantly increased in isolated microglia from microglia-*Lpl*-KD mouse brains; n = 4 per group.
(H) The *Lpl*-KD microglia survival rate (indicated by relative luminescence) is decreased by the glutaminase inhibitor BPTES; n = 7 per group. Data are presented as mean \pm SEM. *p < 0.05, **p < 0.01, ***p < 0.001. Unpaired t test was performed in all experiments. Scale bar, 20 μ m.

suggest that microglial LPL might be involved in the hypothalamic mechanisms that regulates energy metabolism.

Lack of Microglial LPL Disrupts Intracellular Lipid Metabolism

Next, we generated ex vivo primary cultured microglia with a deletion of the *Lpl* gene. Mice carrying loxP-flanked *Lpl* alleles (*Lpl*^{fl/fl}, C57BL/6 background) were crossed with mice carrying tamoxifen-inducible CRE recombinase driven by the *Cx3cr1* promoter (*Cx3cr1*^{CreERT2}, C57BL/6 background). Primary microglia from *Lpl*^{fl/fl}-*Cx3cr1*^{CreERT2} mice were used to generate *Lpl* knockdown microglia (*Lpl*-KD, mixed gender). Primary microglia from *Cx3cr1*^{CreERT2} mice were used as a control (Ctrl). All primary microglia were treated with 4-hydroxytamoxifen to induce deletion of the *Lpl* gene. Successful knockdown (KD) was confirmed by the decrease of *Lpl* mRNA in *Lpl*-KD microglia compared with the Ctrl (Figure 1C).

To test the uptake capacity of TG-rich lipoproteins, *Lpl*-KD microglia and Ctrl cells were incubated with very-low-density lipoprotein (VLDL) particles labeled with the fluorescent dye Dil (VLDL-Dil), which can be taken up by hypothalamic microglia (Valdearcos et al., 2014). Abundant Dil signals were detected in Ctrl microglia but not in *Lpl*-KD microglia (Figures 1D and 1E), indicating a significant downregulation of lipid uptake in *Lpl*-KD microglia.

Subsequently, we found a significant decrease in major phospholipid species, including glycerophosphoethanolamines, glycerophosphocholines, and glycerophosphoinositols, in *Lpl*-

KD microglia (Figures S1A–S1C), suggesting a disrupted intracellular lipid metabolism in microglia that lack LPL.

Microglia Lacking LPL Shift Mitochondrial Fuel Utilization to Glutamine

To investigate whether the changes in intracellular lipid metabolism in *Lpl*-KD microglia affect the fuel utilization by these cells, we examined the oxidative substrate preference of microglia by a mitochondrial fuel flex assay. In this assay, inhibitors were added in a different order and in pre-designed combinations to calculate dependency on glucose, fatty acid, and glutamine oxidation from the changes in oxygen consumption rate (OCR). Glucose and total fatty acid dependencies were not significantly changed in *Lpl*-KD microglia (Figure 1F; Figures S1D and S1E), although fatty acid dependency showed a trend toward decrease in *Lpl*-KD microglia. Interestingly, glutamine dependency was significantly increased in *Lpl*-KD microglia (Figure 1F; Figure S1F). We also found that glutamine synthetase gene expression was elevated in microglia isolated from microglial *Lpl*-KD adult mouse brain compared with those from Ctrl mouse brains (Figure 1G). Glutamine synthetase is an enzyme that catalyzes the formation of glutamine from glutamate. Consistently, by visualizing *glutamate* aspartate transporter (GLAST)-EGFP in GLAST^{CreERT2}-tdTomato-EGFP mice (García-Cáceres et al., 2016), we found GLAST gene expression in microglia (Figures S1G–S1J), confirming that glutamine can be synthesized from intracellular glutamate. However, we also found that the total cellular glutamine and glutamate levels did

not change in *Lpl*-KD microglia (Figures S1K and S1L), suggesting a higher turnover of the glutamine-glutamate cycles in these cells. Thus, *Lpl*-KD microglia are able to shift their fuel utilization to glutamine to compensate for the reduced utilization of fatty acids. We then found that inhibition of glutaminase by *N,N'*-[thiobis(2,1-ethanediyl-1,3,4-thiadiazole-5,2-diyl)] bisbenzeneacetamide (BPTES) resulted in a significant decrease in primary microglial survival rates in *Lpl*-KD microglia (Figure 1H), implying an essential role of glutamine-derived glutamate for cell survival under *Lpl*-KD conditions.

To further confirm these results, we used a fluorescent glucose analog, 2-deoxy-2-[(7-nitro-2,1,3-benzoxadiazol-4-yl) amino]-D-glucose (2-NBDG), to evaluate microglial glucose uptake. With 10 min of 2-NBDG incubation in primary microglia at a concentration of 10 μ M, we found no differences between *Lpl*-KD microglia and Ctrl microglia (Figures S1M and S1N). Also, we detected no differences in gene expression of *Glut1* and *Glut5* between microglia isolated from microglial *Lpl*-KD and Ctrl mouse brains (Figure S1O). Together with our OCR measurements, these findings indicate that cellular glucose metabolism was not significantly affected in microglia lacking LPL.

Microglia Lacking LPL Show Attenuated Immune Response and Phagocytic Capacity

To evaluate microglial immune reactivity in response to immune challenges, we treated microglia with lipopolysaccharide (LPS). We found that tumor necrosis factor alpha (TNF- α) gene expression was significantly lower in *Lpl*-KD microglia (Figure S2A). Because high-fat-diet-derived fatty acids have been found to be one of the major stimuli for microglial activation (Valdearcos et al., 2014), we measured the microglial immune response to palmitic acid (PA). *Tnf- α* gene expression in *Lpl*-KD microglia was profoundly decreased compared with Ctrl microglia (Figure S2A). Because TNF- α produced by microglia is a critical autocrine mediator in microglial activation (Kuno et al., 2005), we checked phospho-nuclear factor κ B (NF- κ B) after TNF- α stimulation and found a significant decrease in phospho-NF- κ B in *Lpl*-KD microglia (Figures S2B and S2C). These data indicate an overall attenuated inflammatory response upon pro-inflammatory stimuli in microglia lacking LPL.

To examine whether the attenuated immune response in microglia is associated with changes in their phagocytic capacity, we measured the uptake of microspheres in primary microglia. In *Lpl*-KD microglia, the uptake of microspheres was significantly reduced compared with that of Ctrl microglia (Figures S2D and S2E), indicating that lacking LPL impairs microglial phagocytic capacity.

Generation of an Animal Model with Postnatal Microglia-Specific Deletion of *Lpl*

To further understand the function of microglial pathophysiology in vivo, we generated a mouse model with specific deletion of the *Lpl* gene from brain microglia at the adult stage. The use of the *Cx3cr1*-Cre^{ERT2} mouse model for brain microglia-specific gene modification has been characterized in detail in previous studies (Goldmann et al., 2013; Yona et al., 2013). Briefly, *Lpl*^{fl/fl} mice were crossed with *Cx3cr1*^{CreERT2} mice as described above.

Male *Lpl*^{fl/fl}-*Cx3cr1*^{CreERT2} mice were used for these experiments. After giving tamoxifen to *Lpl*^{fl/fl}-*Cx3cr1*^{CreERT2} mice at 6 weeks of age, the *Lpl* gene was deleted from microglia and blood mononuclear myeloid cells (Figure S2F). Upon tamoxifen withdrawal, within 2–3 weeks, *Lpl* gene-deleted mononuclear myeloid cells in the periphery were replenished with newly generated wild-type mononuclear myeloid cells from the bone marrow, whereas microglia in the brain retained *Lpl* gene KD (microglia-*Lpl*-KD).

To validate *Lpl* gene deletion, total DNA was isolated from brain and blood mononuclear myeloid cells of microglia-*Lpl*-KD and Ctrl mice 4 weeks and/or 10 weeks after tamoxifen injection and used for PCR analysis. After Cre-induced recombination at the flox site spanning *Lpl* exon 1, a delta band of 409 bp appeared in microglia-*Lpl*-KD mouse brains isolated at week 4 after tamoxifen injection (Figure S2G) but not in blood mononuclear myeloid cells of microglia-*Lpl*-KD mice isolated at week 4 after tamoxifen injection (Figure S2G). At week 10 after tamoxifen injection, we also detected the delta band in hypothalamic tissue of microglia-*Lpl*-KD mice (Figure 2A), thus confirming that *Lpl* gene expression was significantly decreased in these microglia compared with those of Ctrl (Figure 2B). Together, these data demonstrate that tamoxifen-induced Cre recombination occurs in microglia and other populations of long-lived myeloid cells in the CNS, including perivascular macrophages that express *Cx3cr1*.

Mice with Microglia-Specific *Lpl* Deletion on an HCHF Diet Show an Exaggerated Metabolic Phenotype

To evaluate the functional significance of LPL in microglia under physiological and hypercaloric diet conditions, we fed microglia-*Lpl*-KD and Ctrl mice a standard chow or an HCHF diet. Interestingly, the body weight gain, food intake, and body composition of chow-diet-fed microglia-*Lpl*-KD mice were similar to that of Ctrl mice (Figures S2H–S2K). On an HCHF diet, microglia-*Lpl*-KD mice had a similar daily food intake as Ctrl (Figure 2C). Also, no differences in food intake were found in fasting-refed tests on an HCHF diet (data not shown). However, microglia-*Lpl*-KD mice had accelerated body weight gain (Figure 2D), which can be attributed to greater fat mass gain (Figure 2E). Glucose intolerance induced by the HCHF diet was exaggerated in microglia-*Lpl*-KD mice compared with Ctrl (Figure 2F). Although locomotor activity did not differ between Ctrl and microglia-*Lpl*-KD mice on a daily basis (Figure 2G), microglia-*Lpl*-KD mice did have lower heat production during the light phase, indicating less energy expenditure during the resting period (Figure 2H). Because food intake was not different between Ctrl and microglia-*Lpl*-KD mice, reduced heat production might be the major cause of the body weight gain (Tschöp et al., 2011). Furthermore, the respiratory exchange rate (RER) was significantly lower in microglia-*Lpl*-KD mice (Figure 2I), indicating that microglia-*Lpl*-KD mice used more lipids as an energy substrate than Ctrl mice, possibly because of their greater adiposity. These data demonstrate that mice with a microglia-specific *Lpl* deletion were unable to maintain the CNS mechanisms that control systemic glucose and energy metabolism at the proper level when on an HCHF diet.

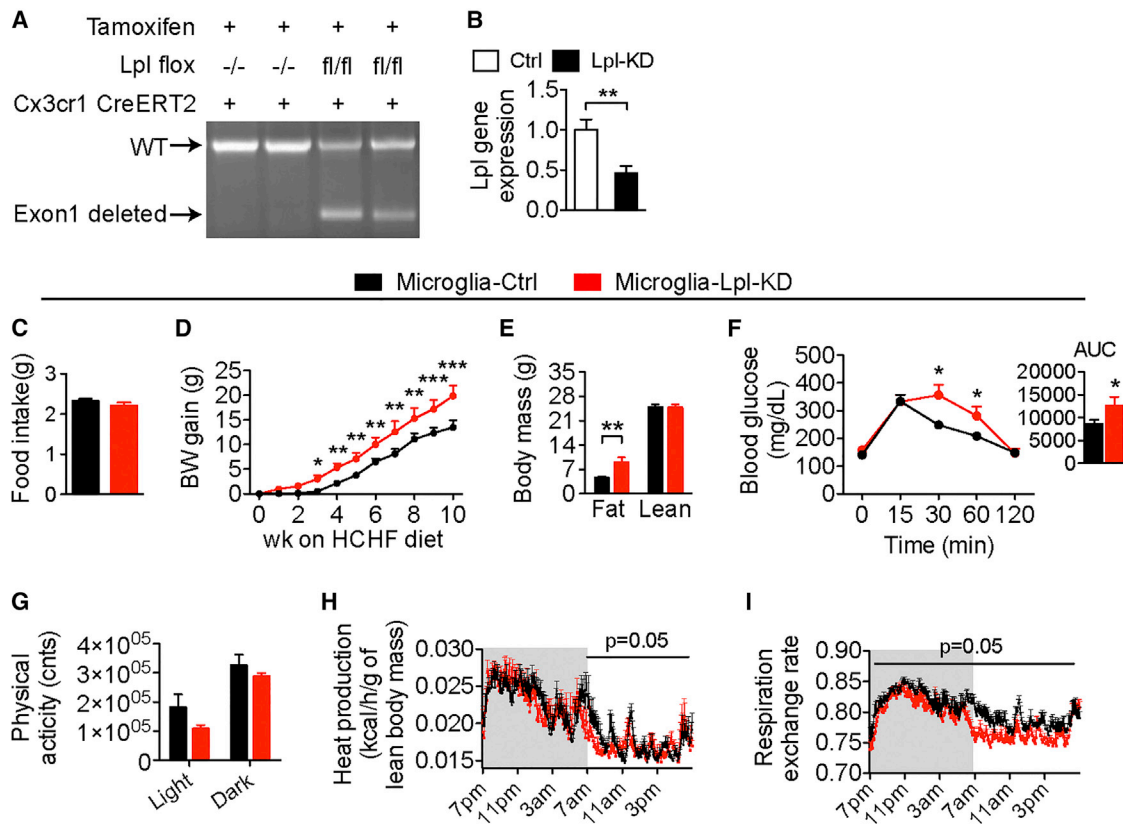


Figure 2. Mice Lacking LPL in Microglia Have Exaggerated Metabolic Disorders on an HCHF Diet

(A) Efficient deletion of the *Lpl* gene is shown by recombined DNA sequence after *Lpl* exon 1 deletion in microglia-*Lpl*-KD mice by PCR in homogenized hypothalamic tissue.
(B) The *Lpl* mRNA level is significantly downregulated in microglia isolated from microglia-*Lpl*-KD mouse brains; n = 6 per group.
(C) Food intake on an HCHF diet does not change in microglia-*Lpl*-KD mice; n = 6–8 per group.
(D) The body weight gain of microglia-*Lpl*-KD mice (n = 11) is significantly greater than that of Ctrl mice (n = 18).
(E) Fat mass is significantly higher in microglia-*Lpl*-KD mice; n = 5–6 per group.
(F) Blood glucose level at 30 and 60 min during a glucose tolerance test are significantly higher in microglia-*Lpl*-KD mice; n = 5–8 per group.
(G) Physical activity does not differ between control and microglia-*Lpl*-KD mice; n = 4 per group.
(H) There is significant lower heat production in microglia-*Lpl*-KD mice during the light phase, n = 4 per group.
(I) There is an effect of genotype on the respiration exchange rate in microglia-*Lpl*-KD mice during the light-dark cycle; n = 4 per group.
Data are presented as mean ± SEM. *p < 0.05, **p < 0.01, ***p < 0.001. Unpaired t test was performed in (D) and (E) and in the area under the curve (AUC) in (F). Two-way ANOVA was performed in (F). Repeated measures ANOVA was performed in (H) and (I).

Microglial Immune Reactivity to an HCHF Diet Is Decreased in the Mediobasal Hypothalamus of Mice with a Microglia-Specific *Lpl* Deletion

To investigate the mechanism behind the metabolic disorders of microglia-*Lpl*-KD mice on an HCHF diet, we examined microglia reactivity in the medial basal hypothalamus (MBH)—the key CNS region regulating systemic energy metabolism. Microglia reactivity was evaluated by iba1 immunoreactivity (iba1-ir). On a standard chow diet, the iba1-ir microglia number, soma size, primary projections, and branching in microglia-*Lpl*-KD mice did not differ from Ctrl mice (Figures S3A–S3E). On an HCHF diet, the iba1-ir microglia number in Ctrl mice was significantly increased compared with that of mice on a chow diet, as we reported previously (Gao et al., 2014). However, iba1-ir microglia number, soma size, primary projections, and branching were significantly decreased in

microglia-*Lpl*-KD mice on an HCHF diet compared with Ctrl mice on an HCHF diet (Figures 3A–3E).

Because phagocytosis represents a key process in microglial immunity (Heneka et al., 2015), we subsequently evaluated the phagocytic capacity of microglia. CD68 was used as the in vivo phagocytic indicator. On a chow diet, we found no differences between microglia-*Lpl*-KD and Ctrl mice (Figures S3F and S3G). However, on an HCHF diet, significantly fewer CD68 ir-positive particles were found in microglia from microglia-*Lpl*-KD mice in comparison with Ctrl mice (Figures 3F and 3G). Consistent with this, we also found CD68 gene expression to be decreased in the MBH of microglia-*Lpl*-KD mice on an HCHF diet (Figure 3H). Thus, deletion of the *Lpl* gene in microglia significantly attenuated microglial reactivity and phagocytic capacity in the MBH when the mice were exposed to an HCHF diet.

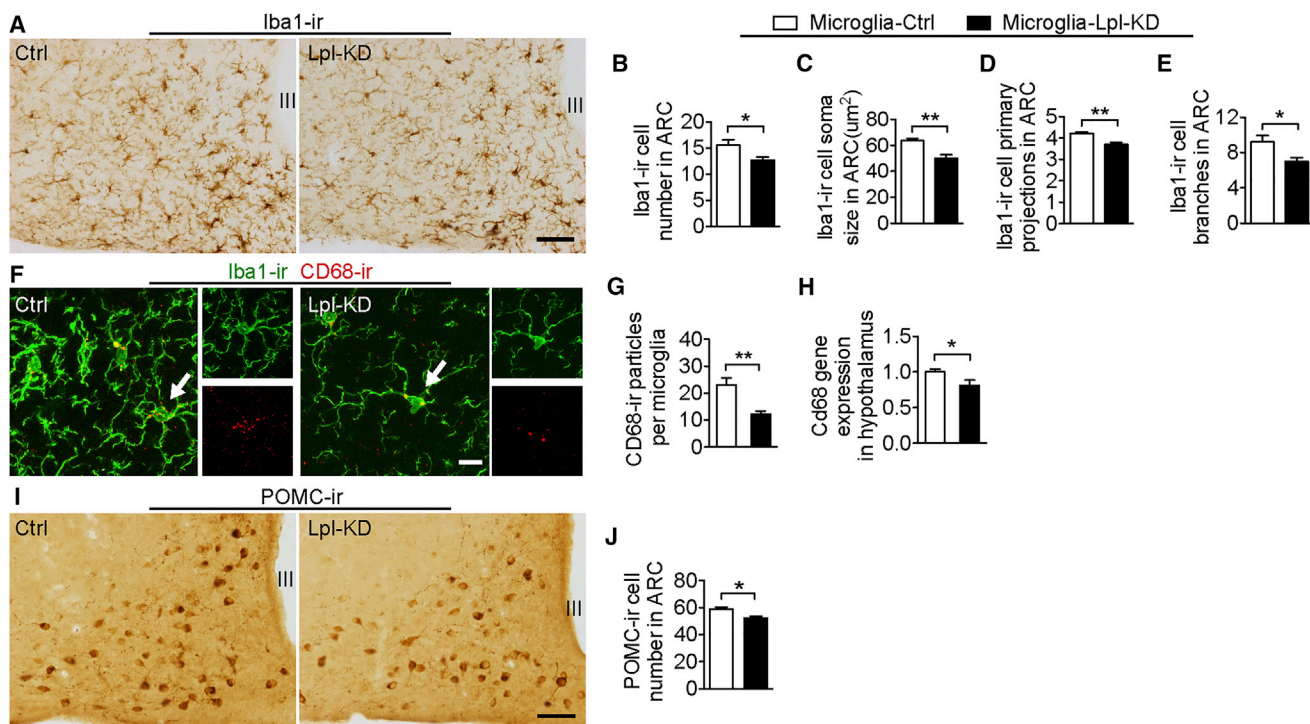


Figure 3. Reduced Microglial Immune Reactivity and Fewer POMC Neurons in the Mediobasal Hypothalamus of Microglia-*Lpl*-KD Mice on an HCHF Diet

(A) Iba1-ir microglia in MBH.

(B–E) The Iba1-ir microglial cell number (B), soma size (C), primary projection (D), and branches (E) are significantly lower in microglia-*Lpl*-KD mouse MBHs on an HCHF diet; n = 7 per group.

(F and G) CD68-ir particles per microglia are significantly lower in microglia-*Lpl*-KD mouse MBHs on an HCHF diet; n = 3–4 per group.

(H) *Cd68* gene expression in HCHF-diet-fed microglia-*Lpl*-KD mouse MBHs are significantly lower; n = 5–7 per group.

(I) POMC-ir in MBH.

(J) The POMC-ir neuronal number is significantly lower in microglia-*Lpl*-KD mouse MBHs on an HCHF diet; n = 7–13 per group.

III, third ventricle. Data are presented as mean ± SEM. *p < 0.05, **p < 0.01. Unpaired t test was performed in all experiments. Scale bars, 100 μm in (A) and (I) and 10 μm in (F).

Diet-induced microglial activation has also been found to be involved in hippocampal dysfunction in memory (Hao et al., 2016). We found that, in Ctrl mice, 10-weeks of the HCHF diet increased Iba1-ir cell branches, but not cell numbers, compared with the chow diet. This increase was significantly reduced in microglia-*Lpl*-KD mice on an HCHF diet (Figure S3H). Thus, our data confirmed that an HCHF diet could impair hippocampus-dependent memory and that this impairment could be affected by deletion of *Lpl* from microglia.

Mice with a Microglia-Specific *Lpl* Deletion Have Accelerated Decrease of POMC Neurons When on an HCHF Diet

Among others, the MBH contains the orexigenic agouti-related peptide (AgRP)-neuropeptide Y (NPY) neurons and anorexigenic proopiomelanocortin (POMC) neurons. Comparing the POMC and NPY neurons, we observed that reactive microglia were more often adjacent to POMC neurons than to NPY neurons (Figures S3I and S3J), as also observed previously (Yi et al., 2017). We therefore examined POMC neurons in the MBH of our microglia-*Lpl*-KD mice. On a chow diet, the

POMC-ir neuron number did not differ between microglia-*Lpl*-KD and Ctrl mice (Figures S3K and S3L), but with an HCHF diet, we observed significantly fewer POMC-ir neurons in microglia-*Lpl*-KD mice compared with Ctrl mice (Figures 3I and 3J).

Microglia-Specific *Lpl* Deletion Results in Mitochondrial Dysfunction in Both Microglia and Nearby Neurons When on an HCHF Diet

Mitochondria are important cellular organelles involved in innate immune signaling pathways (Nakahira et al., 2011; West et al., 2011). To investigate whether the attenuated immunity in *Lpl*-KD microglia is linked to mitochondrial dysfunction, we analyzed the mitochondrial ultrastructure of microglia in the MBH (Figures 4A and 4B).

In comparison with normal mitochondria (Figure 4C1), dysmorphic mitochondria in MBH microglia were characterized by a lower matrix electron density (Figure 4C2), disrupted crista structure (Figure 4C3), and inclusions (Figure 4C4). On a chow diet, there was a significant increase, from 19% to 40%, of dysmorphic microglial mitochondria in the MBH of

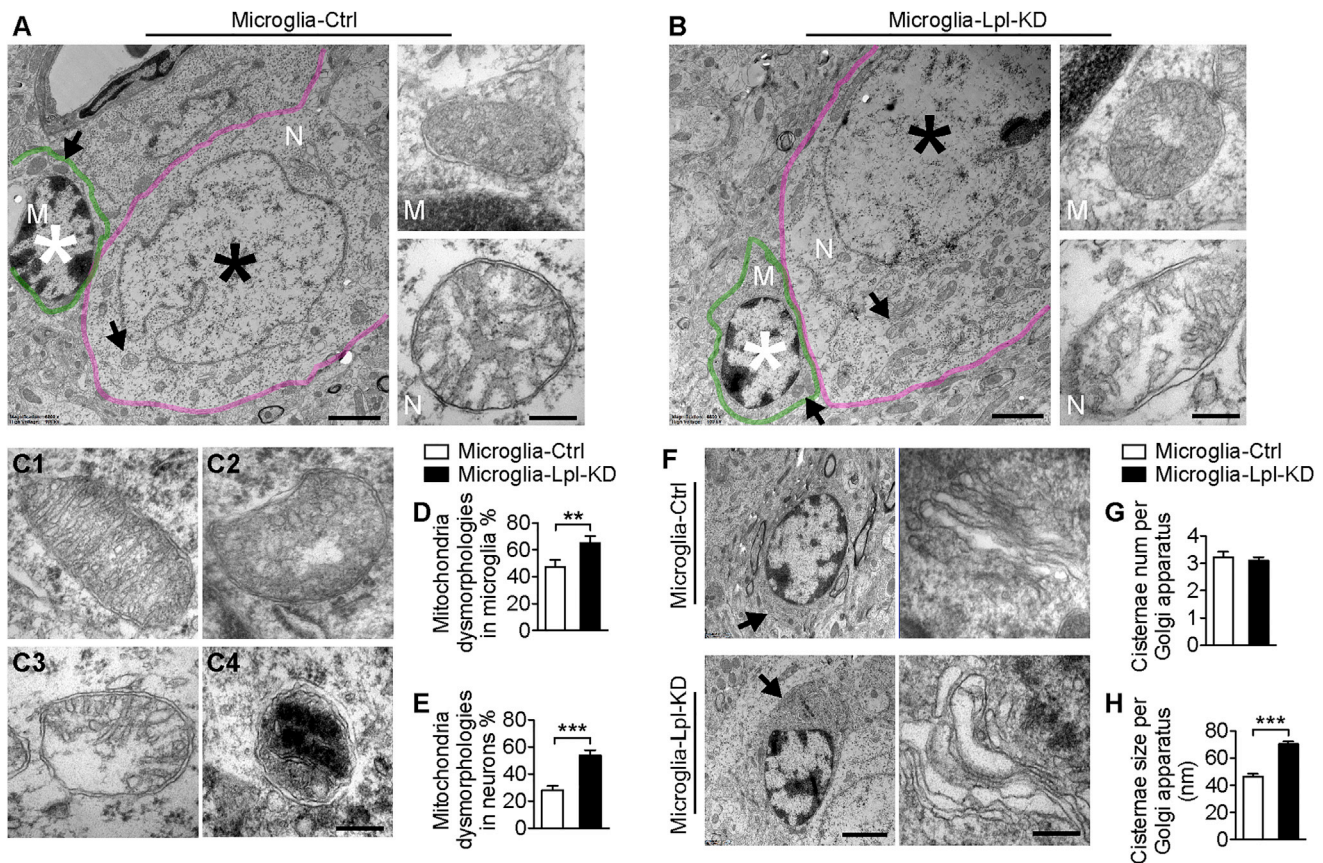


Figure 4. Dysmorphic Mitochondria and Golgi Apparatus in Microglia and Adjacent Neurons in the MBHs of Microglia-Lpl-KD Mice

(A and B) Ultrastructure of mitochondria in microglia (M, outlined by a green line) and adjacent neurons (N, outlined by a pink line) in the MBHs of Ctrl (A) and microglia-Lpl-KD (B) mice fed an HCHF diet. High magnifications of the mitochondrion in each cell (dark arrows) are shown at the right. *, nucleus of each cell. (C1–C4) Normal mitochondrion (C1) and dysmorphic mitochondrion with less electron density (C2), disrupted crista structure (C3), and inclusions (C4).

(D) The dysmorphic mitochondrion ratio in microglia in the MBH is significantly higher in microglia-Lpl-KD mice than in Ctrl mice on an HCHF diet.

(E) The dysmorphic mitochondrion ratio in neurons adjacent to microglia in the MBH is significantly higher in microglia-Lpl-KD mice than in Ctrl mice on an HCHF diet.

(F) Golgi apparatus in microglia in MBH.

(G and H) The average cisterna size (H), but not cisterna number (G), of the Golgi apparatus in microglia in MBH is significantly bigger in microglia-Lpl-KD mice than in Ctrl mice on an HCHF diet. The area indicated by the dark arrow is amplified at the right.

Data are presented as mean \pm SEM. ** $p < 0.01$, *** $p < 0.001$. Unpaired t test was performed in all experiments. Scale bars, 2 μ m in (A) and (B) (left) and (F) (left) and 200 nm in (A) and (B) (right) and (C) and (F) (right).

microglia-Lpl-KD mice in comparison with Ctrl mice (Figures S4A and S4B). On an HCHF diet, we found significantly more dysmorphic mitochondria in MBH microglia in microglia-Lpl-KD mice compared with Ctrl mice (40% in Ctrl versus 65% in Lpl-KD mice; Figures 4A, 4B, and 4D). Moreover, the total number of mitochondria in each microglia per section tended to decrease in microglia-Lpl-KD mice (Figure S4C). Neurons near the microglia exhibited a similar percentage of dysmorphic mitochondria in microglia-Lpl-KD mice and Ctrl mice on a chow diet (Figures S4D–S4F). While on an HCHF diet, we found more dysmorphic mitochondria as well as more autophagosomes in neurons close to microglia in the MBH of microglia-Lpl-KD mice compared with Ctrl mice (Figures 4A, 4B, and 4E; Figures S4G–S4J). Because, upon HCHF diet stimulation, most of the reactive microglia are found adjacent to POMC neurons, we assume that many of

the microglia-adjacent neurons that possess dysmorphic mitochondria are POMC neurons.

Lpl Deletion Induces Swelling of the Golgi Apparatus on an HCHF Diet

Interestingly, we also observed a dysmorphology of another important cell organelle—the Golgi apparatus. On an HCHF diet, the Golgi apparatus in microglia from microglia-Lpl-KD mouse MBH had a significantly larger cisterna size without changes in cisterna number (Figures 4F–4H), indicating a swelling of the microglial Golgi apparatus. The Golgi apparatus processes secretory proteins and lipids and is involved in the endocytic pathway and lysosome formation. Dysfunction of the Golgi apparatus in microglia with Lpl deletion may also contribute to the impaired phagocytic capacity in these cells.

DISCUSSION

Hypothalamic microglia activation is associated with diet-induced obesity (Gao et al., 2014; Thaler et al., 2012). However, whether microglia activation has detrimental effects on hypothalamic neurons is unclear. Here we provide evidence that LPL-regulated intracellular microglia metabolism is important for maintaining microglial immune responses in a hypercaloric environment. LPL seems to be particularly important for supporting its phagocytic capacity, which is fundamental for the clearance of cell debris. LPL is thus a key player in microglial immunometabolism, ensuring the homeostatic brain microenvironment that is necessary for optimal functioning of the neurons in the hypothalamus and other brain regions.

In the CNS, lipid metabolism is quite insulated from the circulation. LPL has been described to translocate to the luminal surface to hydrolyze VLDL in the blood. However, the translocation enzyme glycosylphosphatidylinositol-anchored glycoprotein has been reported to be undetectable in the CNS (Davies et al., 2010). Thus, although LPL is highly abundant in microglia, it might not be translocated through the blood-brain barrier to take up lipoproteins directly from the circulation. In addition, our fasting-refed test on an HCHF diet did not detect any difference between microglia-*Lpl*-KD and Ctrl mice, which also supports that LPL in microglia does not participate directly in the sensing of peripheral lipids. Thus, the majority of the lipoproteins hydrolyzed by microglial LPL are probably produced in the CNS.

Phospholipids are essential components of phagosome formation and remodeling (Boulais et al., 2010). Here we found that, in *Lpl*-KD microglia, the phospholipid content is profoundly reduced, and, concomitantly, the phagocytic capacity is downregulated. Thus, intact LPL-regulated phospholipid homeostasis is required for sufficient microglial phagocytosis. In *Lpl*-KD microglia, glutamine utilization is upregulated. In macrophages, glutamine is important for sustaining inflammatory responses (Rogerio et al., 2010; Wallace and Keast, 1992). Although, in *Lpl*-KD microglia, glutamine utilization was increased, the phospho-NF- κ B response to TNF- α stimulation was downregulated, indicating that microglial immune reactivity might require the presence of both glutamine and lipids.

In neurodegenerative disease, reactive microglia associated with inflammatory agents are considered a major cause of nearby neuronal death (Heneka et al., 2014). During acute neuronal injury, such as that caused by alcohol toxicity, both microglial activation and neurodegeneration are present (Ahlers et al., 2015). In mice that lack neuro-apoptosis, microglial activation is largely abolished. Thus, microglial activation is probably not the cause for the neural injury, but necessary for the removal of dead neurons and tissue recovery. We speculate that a similar microglia-neuron interactive mechanism is operative in microglia-*Lpl*-KD mice. On a chow diet, dysmorphic mitochondria are found in *Lpl*-KD microglia but not in nearby neurons, and the POMC neuron number is intact. This indicates that dysfunctional microglia are not the cause of POMC neuron loss. On an HCHF diet, when metabolic stress is induced, the neural debris generated by POMC neurons exceeds the clearance capacity of *Lpl*-KD microglia because of deficient microglial phagocytic capacity. POMC neurons will retain more dysmorphic mitochondria and other cell debris, as

indicated by an increase in autophagosomes, which might also be in charge of mitochondrial autophagy (mitophagy) and other intracellular pathological processes (Klionsky et al., 2014; Mizushima, 2007). All of these changes might eventually drive POMC neurons to enter a dysfunctional stage.

Previously, we have shown a loss of POMC neurons in wild-type mice after 4 months of HCHF diet (Yi et al., 2017). Our current data suggest that such HCHF-diet-induced POMC neuronal loss is accelerated when the nearby microglia are less reactive because of lack of LPL. α -melanocyte-stimulating hormones (α -MSHs) produced by POMC neurons decrease food intake and increase energy expenditure by binding to melanocortin receptors in discrete downstream areas. Intriguingly, microglia-*Lpl*-KD mice only had reduced heat production, but not increased food intake, as expected from POMC neuronal loss. This raises the possibility that other brain regions inside or outside of the hypothalamus exert inhibitory effects on food intake. Indeed, in microglia-*Lpl*-KD mice, we also observed morphological changes in hippocampal and cortical microglia, both on a chow and/or HCHF diet, indicating that other neural circuits outside of the hypothalamus might be involved in dysregulation of the energy balance. Eventually, the concerted changes inside and outside of the hypothalamic neural circuits resulted in enhanced metabolic disorders in microglia-*Lpl*-KD mice when on an HCHF diet.

Furthermore, the morphological changes in hippocampal and cortical microglia also indicate that cognitive functions in microglia-*Lpl*-KD mice may have changed. This possibility is supported by a recent study in which upregulation of *Lpl* gene expression in a unique cortical microglia population has been identified at an advanced stage of Alzheimer's disease (Keren-Shaul et al., 2017).

At least one remaining question that needs to be answered is how the lipid metabolic disorder caused by the *Lpl* deletion eventually results in mitochondrial dysmorphology. Among the major mitochondrial morphology-regulating genes, we found an upregulation of dynamin-related protein 1 (Drp1) (Figure S4K). Drp1 is a key mediator of mitochondrial fission, and a previous study showed that inhibition of Drp1 blocks cell death (Frank et al., 2001). Whether mitochondrial dysfunction in microglia-*Lpl*-KD mice is linked to increased Drp1 activity will be an important subject for future studies. In the current study, we only investigated the immune response and phagocytic capacity of *Lpl*-KD microglia, taking into account the importance of LPL-gated fatty acid production. Another important question is whether other microglial functions were altered in *Lpl*-KD microglia and can be attributed to part of the observed phenotype. Finally, in the current study, we exclusively studied male mice. Regarding the recent finding that estrogen receptor α regulation of body weight interacts with LPL-dependent lipid processing in the hypothalamus (Wang et al., 2016), it needs to be studied whether female microglia-*Lpl*-KD mice will present different microglial innate immunity in obesity.

EXPERIMENTAL PROCEDURES

Animals

Microglia-specific postnatal *Lpl*-KD mice were generated by crossing *Lpl*^{fl/rt} mice with *Cx3cr1*^{CreERT2} mice (provided by Prof. Steffen Jung, Weizmann

Institute of Science), which harbor the tamoxifen-inducible Cre recombinase driven by the chemokine (C-X3-C motif) receptor 1 (*Cx3cr1*) promoter (Yona et al., 2013). At the age of 6 weeks, tamoxifen was given by intraperitoneal (i.p.) injection for 5 days at a dose of 100 μ g per injection to excise the loxP site of *Lpl*. *Lpl* flox-homozygous and Cre-positive mice (*Lpl^{fl/fl}-Cx3cr1^{CreERT2}*) are referred to as the KD model. Their littermates, which were Cre-positive but had an *Lpl* wild-type sequence, served as Ctrl (*Cx3cr1^{CreERT2}*). All studies were approved by and performed according to the guidelines of the Institutional Animal Care and Use Committee of the Helmholtz Center (Munich, Bavaria, Germany).

Ex Vivo Microglial *Lpl* KD

Primary cells were isolated from neonatal *Lpl^{fl/fl}-Cx3cr1^{CreER}* and *Cx3cr1^{CreER}* mouse brains. When the mixed glial culture reached 90% confluency, L929 cell line conditioned medium was added to the regular modified eagle medium (MEM) (30% v/v) for 2 days to support microglial proliferation. After shaking and seeding, microglia were treated with MEM + 10% fetal calf serum (FCS) + 1% antibiotics + 1 μ M 4-hydroxytamoxifen for 5 consecutive days. Cells were then ready for experiments.

Plate-Based Respirometry

Oxygen consumption rate was recorded by a Seahorse XF analyzer to determine the microglial cellular respiration status. Microglia fuel dependency was tested with a fuel flex test kit (Seahorse Bioscience).

Statistical Analysis

All results are expressed as mean \pm SEM. Statistical comparisons were performed using one-way, two-way, or repeated ANOVA with GraphPad Prism (GraphPad, San Diego, California, USA). Unpaired Student's t test was performed unless indicated otherwise.

SUPPLEMENTAL INFORMATION

Supplemental Information includes Supplemental Experimental Procedures and four figures and can be found with this article online at <http://dx.doi.org/10.1016/j.celrep.2017.09.008>.

AUTHOR CONTRIBUTIONS

Y.G. performed mouse breeding, metabolic phenotyping, primary culture, cell respirometry, PCR, and western blotting. A.V.-I. and N.v.d.W. performed electron microscopy and analyzed the data. M.J.K. performed immunohistochemical and immunofluorescent staining. T.O.E. performed the lipid analysis. C.L., C.G.-C., and J.Y. performed mouse breeding and/or HCHF diet feeding. R.Z.T. performed cell isolation and cell culture. F.M.V., R.H.H., A.J.V., R.H.E., A.K., and S.M.H. provided intellectual input and guidance. C.-X.Y. conceptualized the project, supervised the experiments, interpreted the findings, and drafted the manuscript.

ACKNOWLEDGMENTS

C.X.Y. is supported by an AMC fellowship (2014) and the Dutch Diabetes Fonds (2015.82.1826). We thank Matthias H. Tschöp for intellectual input and Daisy Picavet and Henk van Veen for technical support.

Received: November 13, 2016

Revised: June 28, 2017

Accepted: August 31, 2017

Published: September 26, 2017

REFERENCES

- Ahlers, K.E., Karaçay, B., Fuller, L., Bonthius, D.J., and Dailey, M.E. (2015). Transient activation of microglia following acute alcohol exposure in developing mouse neocortex is primarily driven by BAX-dependent neurodegeneration. *Glia* 63, 1694–1713.
- Babaev, V.R., Fazio, S., Gleaves, L.A., Carter, K.J., Semenkovich, C.F., and Linton, M.F. (1999). Macrophage lipoprotein lipase promotes foam cell formation and atherosclerosis in vivo. *J. Clin. Invest.* 103, 1697–1705.
- Boulais, J., Trost, M., Landry, C.R., Dieckmann, R., Levy, E.D., Soldati, T., Michnick, S.W., Thibault, P., and Desjardins, M. (2010). Molecular characterization of the evolution of phagosomes. *Mol. Syst. Biol.* 6, 423.
- Davies, B.S., Beigneux, A.P., Barnes, R.H., 2nd, Tu, Y., Gin, P., Weinstein, M.M., Nobumori, C., Nyrén, R., Goldberg, I., Olivecrona, G., et al. (2010). GPIIIBP1 is responsible for the entry of lipoprotein lipase into capillaries. *Cell Metab.* 12, 42–52.
- Frank, S., Gaume, B., Bergmann-Leitner, E.S., Leitner, W.W., Robert, E.G., Catez, F., Smith, C.L., and Youle, R.J. (2001). The role of dynamin-related protein 1, a mediator of mitochondrial fission, in apoptosis. *Dev. Cell* 1, 515–525.
- Gao, Y., Ottaway, N., Schriever, S.C., Legutko, B., García-Cáceres, C., de la Fuente, E., Mergen, C., Bour, S., Thaler, J.P., Seeley, R.J., et al. (2014). Hormones and diet, but not body weight, control hypothalamic microglial activity. *Glia* 62, 17–25.
- García-Cáceres, C., Quarta, C., Varela, L., Gao, Y., Gruber, T., Legutko, B., Jastroch, M., Johansson, P., Ninkovic, J., Yi, C.X., et al. (2016). Astrocytic Insulin Signaling Couples Brain Glucose Uptake with Nutrient Availability. *Cell* 166, 867–880.
- Goldmann, T., Wieghofer, P., Müller, P.F., Wolf, Y., Varol, D., Yona, S., Bren-decke, S.M., Kierdorf, K., Staszewski, O., Datta, M., et al. (2013). A new type of microglia gene targeting shows TAK1 to be pivotal in CNS autoimmune inflammation. *Nat. Neurosci.* 16, 1618–1626.
- Hao, S., Dey, A., Yu, X., and Stranahan, A.M. (2016). Dietary obesity reversibly induces synaptic stripping by microglia and impairs hippocampal plasticity. *Brain Behav. Immun.* 51, 230–239.
- Heneka, M.T., Kummer, M.P., and Latz, E. (2014). Innate immune activation in neurodegenerative disease. *Nat. Rev. Immunol.* 14, 463–477.
- Heneka, M.T., Carson, M.J., El Khoury, J., Landreth, G.E., Brosseron, F., Feinstein, D.L., Jacobs, A.H., Wyss-Coray, T., Vitorica, J., Ransohoff, R.M., et al. (2015). Neuroinflammation in Alzheimer's disease. *Lancet Neurol.* 14, 388–405.
- Keren-Shaul, H., Spinrad, A., Weiner, A., Matcovitch-Natan, O., Dvir-Szternfeld, R., Ulland, T.K., David, E., Baruch, K., Lara-Astaiso, D., Toth, B., et al. (2017). A Unique Microglia Type Associated with Restricting Development of Alzheimer's Disease. *Cell* 169, 1276–1290.e17.
- Kettenmann, H., Hanisch, U.K., Noda, M., and Verkhratsky, A. (2011). Physiology of microglia. *Physiol. Rev.* 91, 461–553.
- Klionsky, D.J., Eskelinen, E.L., and Deretic, V. (2014). Autophagosomes, phagosomes, autolysosomes, phagolysosomes, autophagolysosomes... wait, I'm confused. *Autophagy* 10, 549–551.
- Kuno, R., Wang, J., Kawanokuchi, J., Takeuchi, H., Mizuno, T., and Suzumura, A. (2005). Autocrine activation of microglia by tumor necrosis factor- α . *J. Neuroimmunol.* 162, 89–96.
- Li, Y., Du, X.F., Liu, C.S., Wen, Z.L., and Du, J.L. (2012). Reciprocal regulation between resting microglial dynamics and neuronal activity in vivo. *Dev. Cell* 23, 1189–1202.
- Mizushima, N. (2007). Autophagy: process and function. *Genes Dev.* 21, 2861–2873.
- Nakahira, K., Haspel, J.A., Rathinam, V.A., Lee, S.J., Dolinay, T., Lam, H.C., Englert, J.A., Rabinovitch, M., Cernadas, M., Kim, H.P., et al. (2011). Autophagy proteins regulate innate immune responses by inhibiting the release of mitochondrial DNA mediated by the NALP3 inflammasome. *Nat. Immunol.* 12, 222–230.
- Newsholme, P., Curi, R., Gordon, S., and Newsholme, E.A. (1986). Metabolism of glucose, glutamine, long-chain fatty acids and ketone bodies by murine macrophages. *Biochem. J.* 239, 121–125.
- O'Neill, L.A., Kishton, R.J., and Rathmell, J. (2016). A guide to immunometabolism for immunologists. *Nat. Rev. Immunol.* 16, 553–565.
- Oren, R., Farnham, A.E., Saito, K., Milofsky, E., and Karnovsky, M.L. (1963). Metabolic patterns in three types of phagocytizing cells. *J. Cell Biol.* 17, 487–501.

- Prinz, M., and Priller, J. (2014). Microglia and brain macrophages in the molecular age: from origin to neuropsychiatric disease. *Nat. Rev. Neurosci.* **15**, 300–312.
- Rogero, M.M., Borelli, P., Fock, R.A., Borges, M.C., Vinolo, M.A., Curi, R., Nakajima, K., Crisma, A.R., Ramos, A.D., and Tirapegui, J. (2010). Effects of glutamine on the nuclear factor-kappaB signaling pathway of murine peritoneal macrophages. *Amino Acids* **39**, 435–441.
- Thaler, J.P., Yi, C.X., Schur, E.A., Guyenet, S.J., Hwang, B.H., Dietrich, M.O., Zhao, X., Sarruf, D.A., Izgur, V., Maravilla, K.R., et al. (2012). Obesity is associated with hypothalamic injury in rodents and humans. *J. Clin. Invest.* **122**, 153–162.
- Tschöp, M.H., Speakman, J.R., Arch, J.R., Auwerx, J., Brüning, J.C., Chan, L., Eckel, R.H., Farese, R.V., Jr., Galgani, J.E., Hambly, C., et al. (2011). A guide to analysis of mouse energy metabolism. *Nat. Methods* **9**, 57–63.
- Valdearcos, M., Robblee, M.M., Benjamin, D.I., Nomura, D.K., Xu, A.W., and Koliwad, S.K. (2014). Microglia dictate the impact of saturated fat consumption on hypothalamic inflammation and neuronal function. *Cell Rep.* **9**, 2124–2138.
- Wallace, C., and Keast, D. (1992). Glutamine and macrophage function. *Metabolism* **41**, 1016–1020.
- Wang, H., and Eckel, R.H. (2009). Lipoprotein lipase: from gene to obesity. *Am. J. Physiol. Endocrinol. Metab.* **297**, E271–E288.
- Wang, H., Wang, Y., Taussig, M.D., and Eckel, R.H. (2016). Sex differences in obesity development in pair-fed neuronal lipoprotein lipase deficient mice. *Mol. Metab.* **5**, 1025–1032.
- West, A.P., Shadel, G.S., and Ghosh, S. (2011). Mitochondria in innate immune responses. *Nat. Rev. Immunol.* **11**, 389–402.
- Yi, C.X., Walter, M., Gao, Y., Pitra, S., Legutko, B., Kälén, S., Layritz, C., García-Cáceres, C., Bielohuby, M., Bidlingmaier, M., et al. (2017). TNF α drives mitochondrial stress in POMC neurons in obesity. *Nat. Commun.* **8**, 15143.
- Yona, S., Kim, K.W., Wolf, Y., Mildner, A., Varol, D., Breker, M., Strauss-Ayali, D., Viukov, S., Guillems, M., Misharin, A., et al. (2013). Fate mapping reveals origins and dynamics of monocytes and tissue macrophages under homeostasis. *Immunity* **38**, 79–91.
- Zhang, Y., Chen, K., Sloan, S.A., Bennett, M.L., Scholze, A.R., O’Keeffe, S., Phatnani, H.P., Guarnieri, P., Caneda, C., Ruderisch, N., et al. (2014). An RNA-sequencing transcriptome and splicing database of glia, neurons, and vascular cells of the cerebral cortex. *J. Neurosci.* **34**, 11929–11947.
- Zhang, Y., Sloan, S.A., Clarke, L.E., Caneda, C., Plaza, C.A., Blumenthal, P.D., Vogel, H., Steinberg, G.K., Edwards, M.S., Li, G., et al. (2016). Purification and Characterization of Progenitor and Mature Human Astrocytes Reveals Transcriptional and Functional Differences with Mouse. *Neuron* **89**, 37–53.

Supplemental Information

Lipoprotein Lipase Maintains Microglial

Innate Immunity in Obesity

Yuanqing Gao, Andrés Vidal-Itriago, Martin J. Kalsbeek, Clarita Layritz, Cristina García-Cáceres, Robby Zachariah Tom, Thomas O. Eichmann, Frédéric M. Vaz, Riekelt H. Houtkooper, Nicole van der Wel, Arthur J. Verhoeven, Jie Yan, Andries Kalsbeek, Robert H. Eckel, Susanna M. Hofmann, and Chun-Xia Yi

Supplemental Information

Lipoprotein lipase maintains microglial innate immunity in obesity

Yuanqing Gao, Andrés Vidal-Itriago, Martin J. Kalsbeek, Clarita Layritz, Cristina García-Cáceres, Robby Zachariah Tom, Thomas O Eichmann, Frédéric M. Vaz, Riekelt H Houtkooper, Nicole van der Wel, Arthur J. Verhoeven, Jie Yan, Andries Kalsbeek, Robert H. Eckel, Susanna M. Hofmann, Chun-Xia Yi

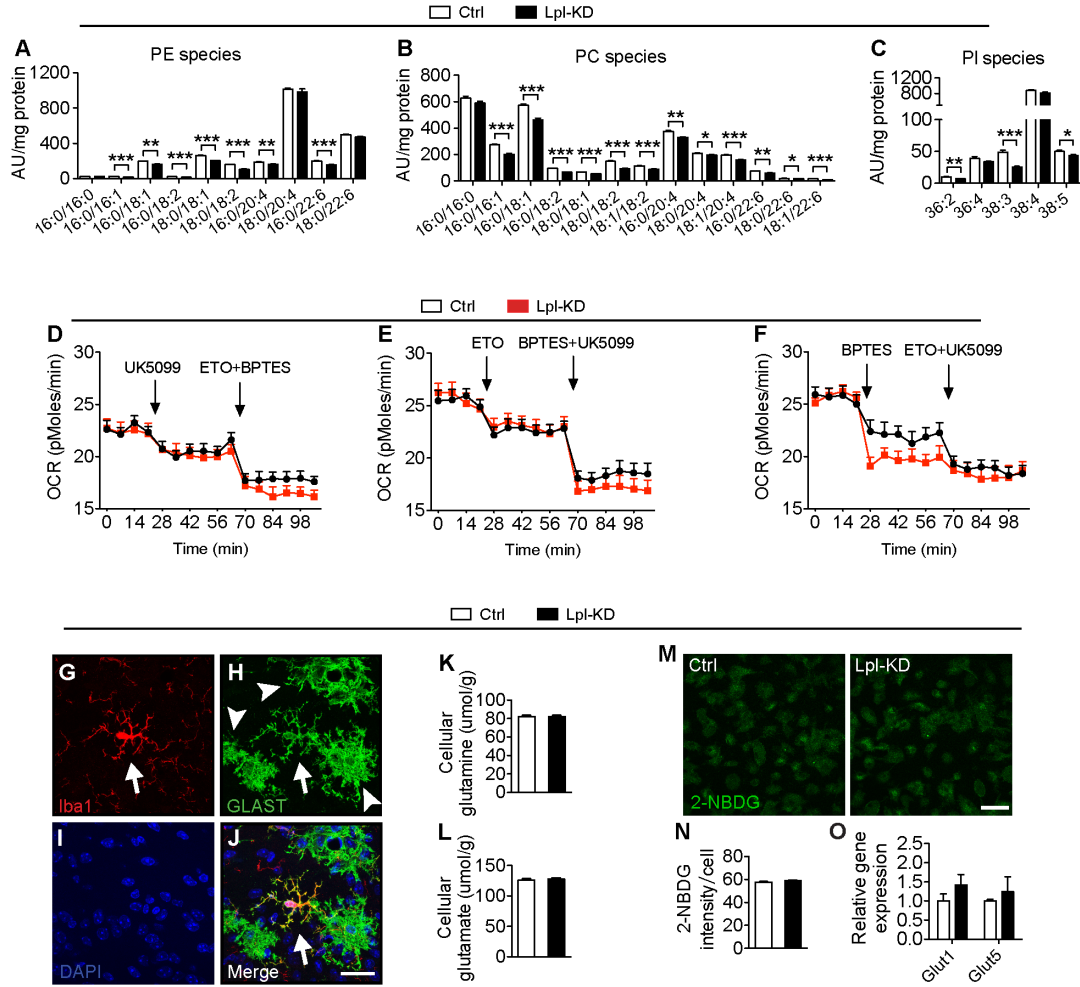


Figure S1. *Lpl*-KD microglial phospholipids contents and fuel utilizations. Related to Figure 1. (A-C) Control and *Lpl*-KD primary microglia phospholipids profiles, including glycerophosphoethanolamines (PE) species (A), glycerophosphocholines (PC) species (B) and glycerophosphoinositols (PI) species (C), $n=4$ per group, AU: arbitrary units. (D-F) Fuel Flex test on glucose (D), fatty acids (E) and glutamine (F) dependency in *Lpl*-KD microglia. UK-5099: 2-Cyano-3-(1-phenyl-1H-indol-3-yl)-2-propenoic acid, BPTES: *N,N'*-[Thiobis(2,1-ethanediyl-1,3,4-thiadiazole-5,2-diyl)] bisbenzeneacetamide, ETO: Etomoxir. (G-J) Iba1-ir microglial cells (pointed by arrows in G, H and J) express GLAST gene (visualized by eGFP in $GLAST^{CreERT2}$ -tdTomato-eGFP mice received tamoxifen injection), notice the GLAST-eGFP in the astrocytes near the Iba1-ir microglia, pointed by arrowheads in H). (K&L) Intracellular glutamine and glutamate concentration do not differ between primarily cultured control microglia and *Lpl*-KD microglia. (M&N) 2-deoxy-2-[(7-nitro-2,1,3-benzoxadiazol-4-yl) amino]-D-glucose (2-NBDG) uptake do not differ between primarily cultured control microglia and *Lpl*-KD microglia, $n=8-9$ per group. (O) Gene expression of *Glut1* and *Glut5* in microglia isolated from control and microglia-*Lpl*-KD mouse brains are similar, $n=4$ per group. Data are presented by mean \pm SEM. * $p<0.05$, ** $p<0.01$, *** $p<0.001$. Unpaired t-test was performed in all experiments. Scale bar: 25 μ m in G-J, 20 μ m in M.

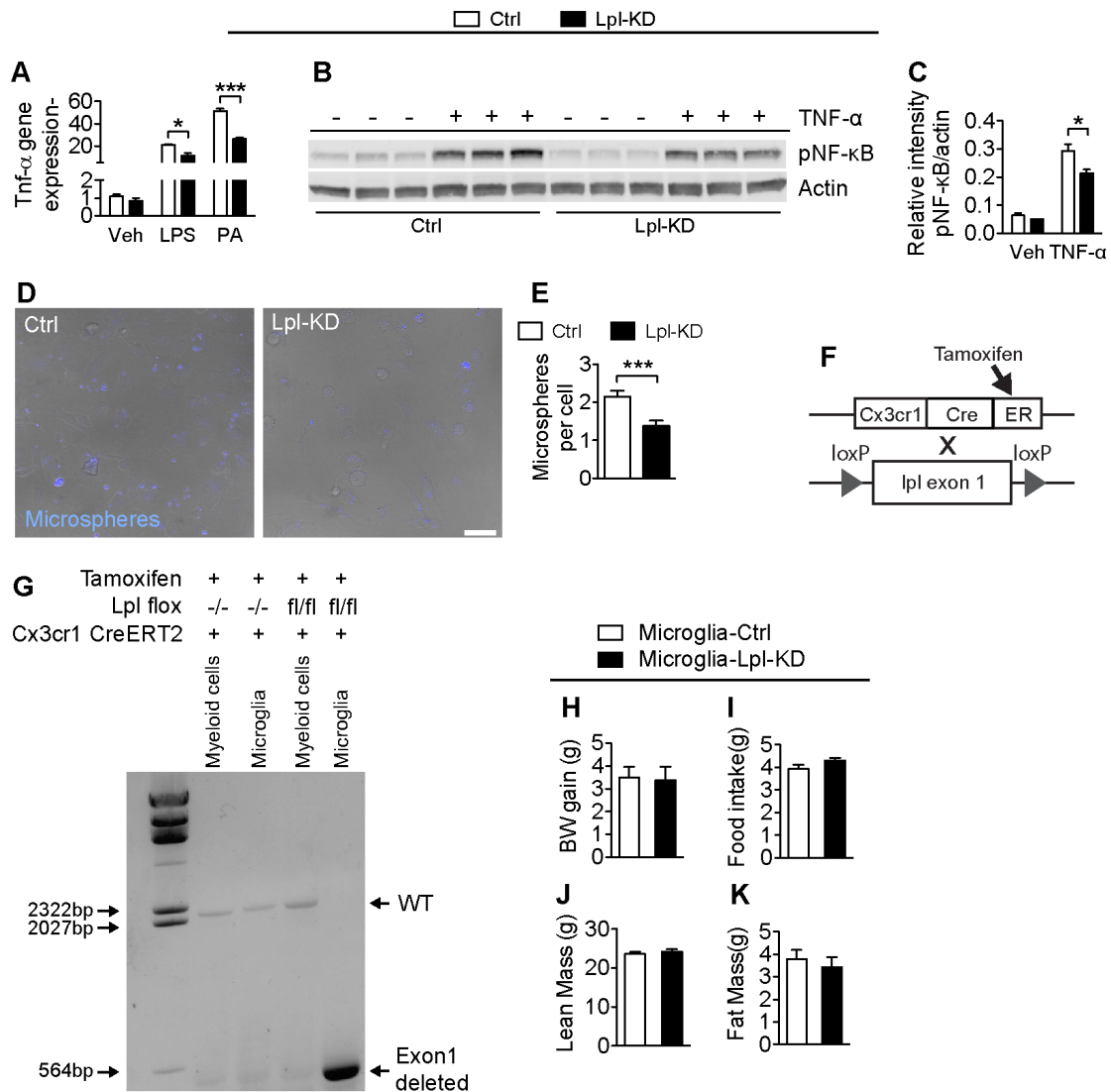


Figure S2. Immune reactivity of *Lpl*-KD microglia and metabolic phenotype of control and microglia-*Lpl*-KD mice on standard chow diet. Related to Figure 1 and Figure 2.

(A) *Tnf-α* gene expression in *Lpl*-KD microglia is significantly less than in control microglia in response to lipopolysaccharides (LPS) and palmitic acid (PA) stimulation. (B&C) Immunoblot of phosphor-NF-κB in response to TNF-α is significantly lower in *Lpl*-KD microglia. (D&E) The uptake of microspheres by *Lpl*-KD microglia is significantly down regulated. (F) Mice breeding strategy for postnatal deletion of *Lpl* gene specifically from microglia. (G) Four weeks after tamoxifen injection, recombinant DNA sequence after *Lpl* exon1 deletion can be detected in microglia isolated from microglia-*Lpl*-KD mouse brain, but not detectable in control mouse microglia, neither in peripheral mononuclear myeloid cells isolated from control mice nor microglia-*Lpl*-KD mice. (H-K) Metabolic phenotypes do not differ between control and microglia-*Lpl*-KD mice fed on standard chow diet, shown by (H) bodyweight gain (at 20 weeks of the age), (I) averaged daily food intake, (J) lean mass and (K) fat mass, n=4-6 per group. Data are presented by mean ± SEM. * $p < 0.05$, *** $p < 0.001$. Scale bar: 30 μm in D.

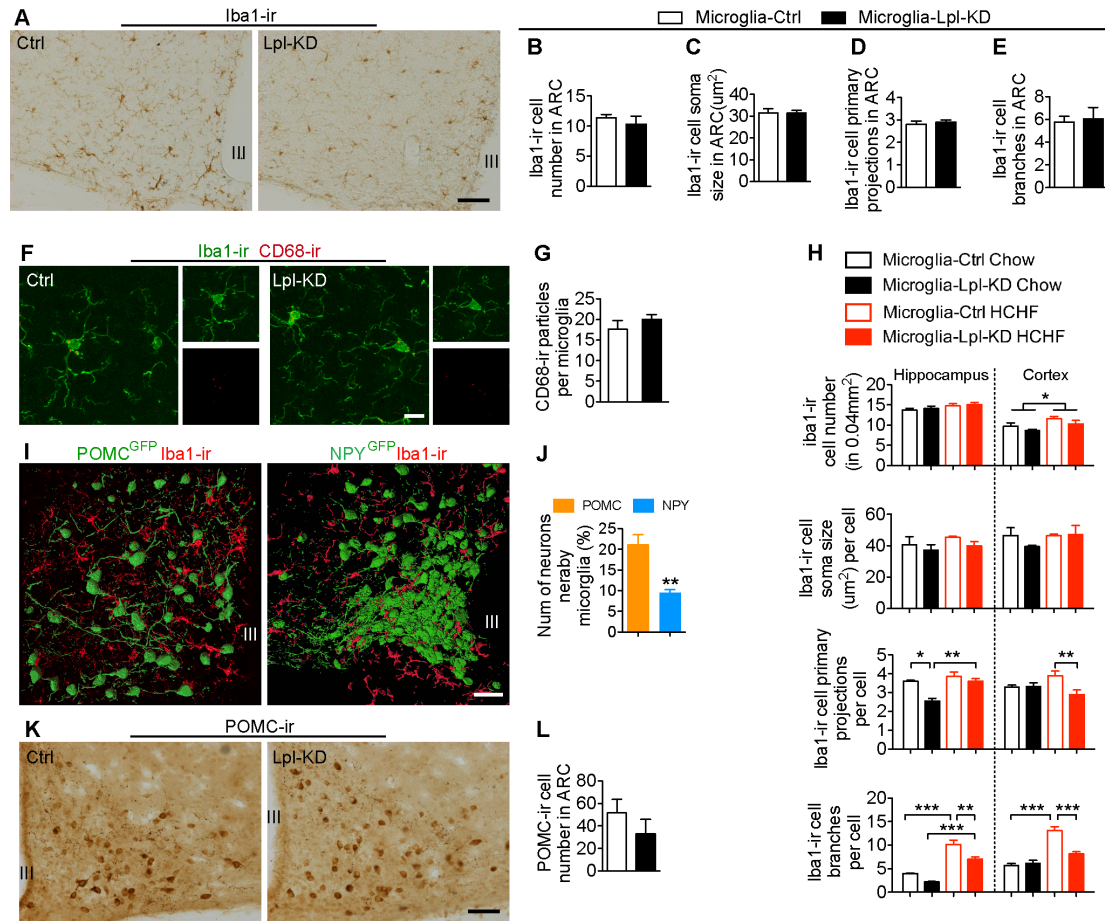


Figure S3. Microglial immune reactivity and POMC neurons are not changed in the mediobasal hypothalamus of microglia-*Lpl*-KD mice on standard chow diet. Related to Figure 3.

(A-E) Iba1-ir microglial number, soma size, primary projection and branches in ARC in the mediobasal hypothalamus do not differ between control and microglia-*Lpl*-KD mice on chow diet, $n=3-4$ per group. (F&G) CD68-ir particles per microglia are similar between control and microglia-*Lpl*-KD mice on chow diet, $n=4-5$ per group. (I&J) Microglia have higher affinity with POMC neuron than with NPY neurons on HCHF diet. (K&L) POMC-ir neuronal number is similar between control and microglia-*Lpl*-KD mice on chow diet, $n=3-4$ per group. (H) Iba1-ir microglial number, soma size, primary projection and branches in hippocampus and cortex differ between control and microglia-*Lpl*-KD mice on chow or HCHF diets, $n=3-7$ per group. III: third ventricle. Data are presented by mean \pm SEM. * $p<0.05$, ** $p<0.01$, *** $p<0.001$. Scale bar: 50 μm in A and I, 10 μm in F, 100 μm in K.

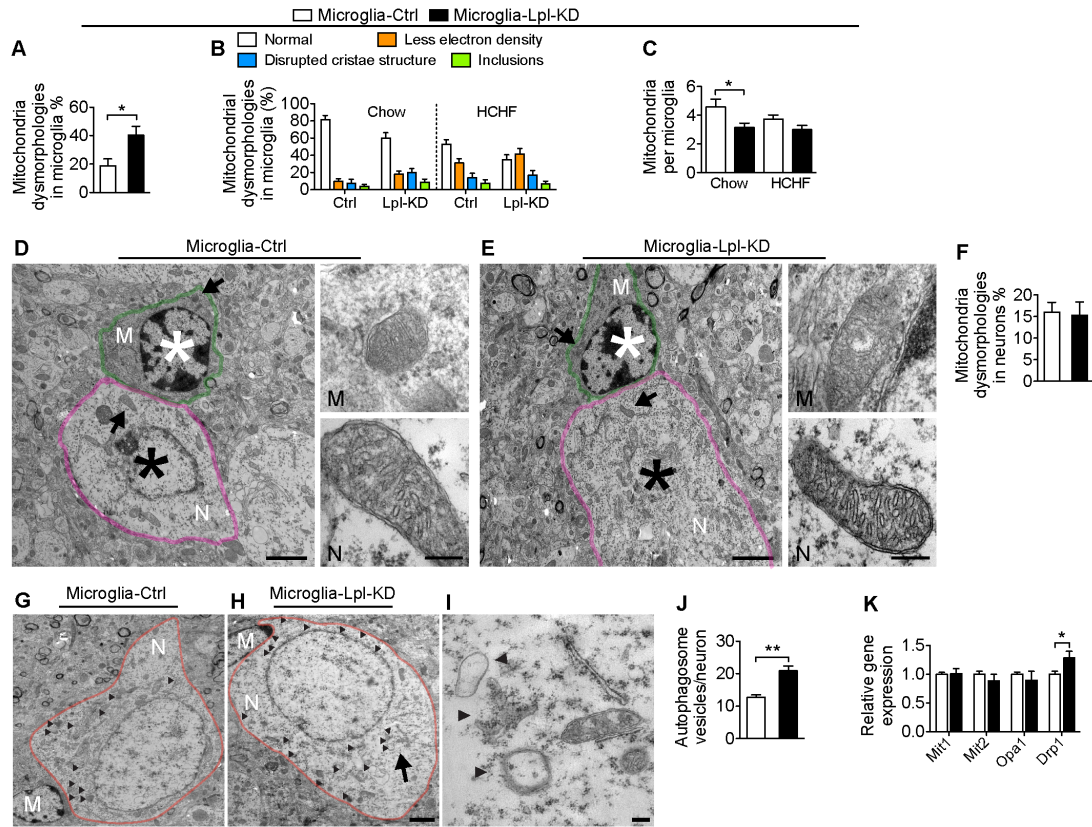


Figure S4. Dysmorphic mitochondria increase in microglia but not in nearby neurons in the mediobasal hypothalamus of microglia-*Lpl*-KD mice on standard chow diet. Related to Figure 4. (A) Dysmorphic mitochondria ratio in microglia in MBH is significantly higher in microglia-*Lpl*-KD mice than in control mice on standard chow diet. (B) Dysmorphic mitochondria ratio classified by lower electron density, disrupted cristae structure and inclusions in microglia in the MBH of microglia-*Lpl*-KD mice on both standard chow diet and HCHF diet. (C) Visible mitochondrial number per microglia is less in microglia-*Lpl*-KD mice MBH on standard chow diet, and tend to decrease on HCHF diet. (D & E) Ultrastructure of mitochondria in microglia (M, outlined by green line) and adjacent neuron (N, outlined by pink line) in the MBH of control mice (D) and microglia-*Lpl*-KD mice (E) on standard chow diet. High magnifications of dark arrows pointed mitochondrion in each cell are amplified in the right panels. *: Nucleus of each cell. (F) Dysmorphic mitochondria ratio in neurons adjacent to microglia in MBH is similar between microglia-*Lpl*-KD mice and control mice on standard chow diet. (G,H&J) Autophagosomes (pointed by black arrow head) in MBH neurons (N, outlined by red line) nearby the *Lpl*-KD microglia (M) (n=10 neurons) are significantly more than in control mice (n=8 neurons). The area pointed by arrow in H is amplified in I. Data are presented by mean \pm SEM. * $p < 0.05$. ** $p < 0.01$. Scale bar: (K) Drp1 gene expression is higher in primarily cultured *Lpl*-KD microglia. Data are presented by mean \pm SEM. Unpaired t-test was performed in all experiments. Scale bar: left panel of D and E: 2 μ m, G and H: 2 μ m, right panel of D and E: 200 nm, I: 200 nm.

Supplemental experimental procedures

Animals

All studies were approved by and performed according to the guidelines of the Institutional Animal Care and Use Committee of the Helmholtz Center Munich, Bavaria, Germany. POMC-eGFP and NPY-eGFP mouse strains were from Jackson Laboratory breeding on C57BL/6 background. For visualizing glutamate aspartate transporter (GLAST)-eGFP, GLAST^{CreERT2} - tdTomato-eGFP mice were generated and injected with tamoxifen as previously described (Garcia-Caceres et al., 2016).

All mice were group housed on a 12/12-hours light dark cycle at 23°C, with free access to food and water. Mice were fed either a standard chow diet (LM-485, Harlan Teklad), or a high carbohydrate high fat (HCHF) diet of which 58% kcal was fat (D12331; Research Diets, New Brunswick, NJ) for 10 weeks from the age of 10 week. Mice fed on a HCHF diet for 10 weeks were used for co staining with iba1.

Metabolic phenotyping of control and microglia-*Lpl*-KD mice

Bodyweight and food intake were monitored throughout the whole study. Food intake was calculated on a weekly basis. Whole-body composition (fat and lean mass) was measured using nuclear magnetic resonance technology (EchoMRI-100; Echo Medical Systems). RER, locomotor activity and heat production were measured by a customized indirect gas calorimetric system at week 10 after tamoxifen injection (TSE Systems GmbH, Bad Homburg, Germany). In short, chow diet or HCHF diet-fed mice were single housed in metabolic cage equipped with PhenoMaster module for indirect gas calorimetry for three days for adaptation, afterward, a continuous 24 hours of measurements of oxygen consumption (VO₂) and carbon dioxide production (VCO₂) were used for calculating respiratory exchange rate, heat production and substrate utilization (fat reserves vs. carbohydrate catabolism). Heat production was normalized by lean body mass.

Primary microglia culture

Brain tissues were isolated from neonatal mice and triturated in MEM (Life Technologies, CA) containing 1% penicillin-streptomycin, 10% fetal calf serum (FCS; life Technologies) and 5.5 mM glucose. The cell suspension was centrifuged for 5 min at 1000 rpm and the pellet was re-suspended and seeded in a 175-cm³ cell culture flasks. Cells were incubated at 37°C and 5% CO₂ for 9 days with MEM containing 10% FCS and 1% antibiotics. Medium was changed every 3 days. When mixed glial culture reach 90% confluency, L929 cell line conditioned medium was added into the regular MEM (30% v/v) and incubated with cells for 2 days to stimulate microglia proliferation. When microglia become confluent, flasks were placed in a 37°C shaker at 150 rpm for 1 hour to detach microglia. After shaking, medium was collected and passed through 40 µm filters. After centrifugation for 5 min at 380 g, the cell pellet was re-suspended in MEM + 10% FCS + 1% antibiotics and seeded for experiments. For lipopolysaccharides (LPS) and palmitic acid treatment, primary microglia were incubated with serum-free MEM medium with 1 µg/ml LPS or 50 µM palmitic acid (BSA conjugated) for 16 hours, serum-free MEM medium was used as the vehicle control. After 3 times wash with PBS, cells were harvested for analysis.

Microglia isolation from adult brain tissue

For hypothalamic microglial isolation, mice were decapitated and brains were isolated, hypothalami were dissected out according to the mouse brain atlas (Paxinos and Franklin 2008). Fresh hypothalamic tissues were gently homogenized in RPMI (21875-034, Gibco) medium in the hand homogenizer. After 5 min centrifugation at 380 g at 4 degrees, cells were re-suspended with 7 ml RPMI and mixed with 3 ml 100% Percoll solution (p1644, sigma). Cell suspension was then layered slowly onto the top of 2 ml 70% Percoll solution in a new 15 ml falcon and centrifuged at 500 g speed for 30 min at 18 degrees, with accelerate and break rate at 1. After centrifugation, the fuse interphases were transferred into a new 15 ml falcon with 8 ml HBSS (14170112, Gibco) and centrifuged at 500 g for 7 min again. Cells were then incubated with CD11b antibody coated microbeads (130-097-059, Miltenyl Biotec) for 30 min at 4 degrees. CD11b positive microglia were further purified by passing through MACS Columns (130-042-201, Miltenyl Biotec) by magnetic separation.

Blood mononuclear myeloid isolation

Circulating mononuclear cells were isolated from the blood collected from Ctrl or *Lpl*-KD mice. Red blood cells were removed by red blood cell lysis solution (130-94-183, Miltenyl Biotec). After centrifuging, the rest of the cells were re-suspended in 5 ml RPMI medium and layered on top of 5 ml Ficoll (17-1440-02, GE healthcare) solution slowly in a new 15 ml falcon. After centrifuging with 400

g at 20 degrees for 30 min (break 1/1), the fuse interphase was transferred into a new 15 ml falcon and filled up with 8 ml HBSS. After 5 min centrifugation with 200 g at RT, the cells were seeded into culture plate with RPMI. After 30 min, floating cells were washed away and attached mononuclear cells were harvested for PCR analysis.

Glucose Tolerance Test

An intraperitoneal glucose tolerance test (ipGTT) was performed by injection of glucose (2 g/kg, 25% wt/vol. D-glucose (Sigma, Germany) in 0.9% wt/vol NaCl after a 5-hours fast. Tail blood glucose levels (mg/dl) were measured with a TheraSense Freestyle glucometer (Abbott Diabetes Care, Inc., Alameda, CA) before (0 min) and at 15, 30, 60 and 120 min after injection.

Lipid and Glucose uptake assay

To determine the lipid uptake capacity, 5 ug/ml Dil labeled VLDL particles were incubated with primary microglia in the culture for 1 hour at 37 degrees. Cells were washed with PBS for 3 times and fixed with 1% paraformaldehyde for 10 min before confocal imaging.

To determine the glucose uptake capacity, 2-deoxy-2-[(7-nitro-2,1,3-benzoxadiazol-4-yl) amino]-D-glucose (2-NBDG) was incubated with primary microglia for 10 min at 37 degrees with a concentration of 10 μ M. Cells were washed with PBS for 3 time and kept in PBS for live imaging by confocal microscope.

Fuel flex assay

Microglia were seeded in an XF96 plate with 100,000 cells per well (Seahorse Bioscience, North Billerica, MA, USA). After 4-Hydroxytamoxifen treatment for 5 days, cells were washed with PBS and incubated with XF assay medium containing 5.5 mM glucose, 2 mM glutamine and 1 mM pyruvate for 1 hour in a 37°C air incubator. The XF96 plate was then transferred to a temperature-controlled (37°C) extracellular flux analyzer (Seahorse Bioscience) and subjected to an equilibration period. Each assay cycle consisted of a 3-min mix and 3-min measure period. Oxygen consumption rate was recorded during the assay to determine the cellular respiration status. Microglia fuel dependency was tested by fuel flex test kit (Seahorse bioscience). All the compounds were included in the kit and diluted with XF assay medium. Assay details were described in the kit. Briefly, after 4 basal assay cycles, 3 inhibitors were added in different order by automatic pneumatic injection to test the fuel dependency of the cells. To determine glucose dependency, UK-5099 (2-Cyano-3-(1-phenyl-1H-indol-3-yl)-2-propenoic acid) was injected from port A to inhibit pyruvate-dependent O₂ consumption. After 6 assay cycles, BPTES and Etomoxir were injected from port B to inhibit glutaminase and long chain fatty acids oxidation. To determine glutamine dependency, BPTES was injected from port A and UK-5099, Etomoxir were injected from port B. To determine fatty acids oxidation, Etomoxir was injected from port A, BPTES and UK-5099 were injected from port B.

Microglia viability assay

To examine the glutamine dependency of *Lpl*-KD microglia, microglia survival rates were measured by CellTiter-Fluor™ Cell Viability Assay (G6080, Promega) with glutamine deprivation medium or glutaminase inhibitor BPTES treatment for 4 hours in control or *Lpl*-KD primary cultured microglia.

Phagocytosis assay

Microspheres (1 μ m, Fluoresbrite® BB Carboxylate, poly science) were coated with PBS-containing 10%FBS at 37 °C for 1 hour. Coated beads were centrifuged and re-suspended in PBS. Coated microspheres were added into the primary cultured control or *Lpl*-KD microglia (1000 microspheres per cell), 1 hour later, cells were washed 3 times with PBS and fixed by 4% paraformaldehyde for confocal imaging. Microspheres per cell were manually counted in each well, 5 wells per group.

Gene expression analysis

For gene expression analysis, hypothalamic tissue was harvested and total RNA was isolated by an RNeasy lipid tissue kit (Qiagen, Germany). After reverse transcription by a QuantiTect Rev. Transcription Kit (Qiagen, Germany), gene expression was analyzed by a real-time PCR with either Taqman probes (Applied Biosystems) and or SYBR primers. *Lpl*: Mm00434764_m1; *Glul*: Mm00725701_s1; *TNF- α* : Mm00443258_m1; *Cd68*: Forward 5'-CTTGTGTTTCAGCTCCAAGCC-3'; Reverse: 5'- GATGGGTACCGTCACAACCT-3'. *Mit1*: Forward 5'-GGATAAAGTCCTCCCCAGCG-3'; Reverse: 5'- GCATGGGCCAGCTGATTAAC-3'. *Mit2*: Forward 5'- GGACCTCCATGGGCATTCTT-3'; Reverse: 5'- CTGTAGCTTCTCACTGGCGT-3'. *Opal*: Forward 5'-GGACCTCCATGGGCATTCTT-3'; Reverse: 5'- GCTTCCGCAGCTCTTTGTTC-3'. *Drp1*:

Forward 5'-TGACCCTGCCACATGGAAAA-3'; Reverse: 5'-TGGATTGGCTCAGGGCTTAC-3'. Hypoxanthine phosphoribosyltransferase 1 (HPRT) was used as a housekeeping gene (Mm01545399_m1 for taqman assay or following primer set for SYBR: Forward 5'-GCAGTACAGCCCCAAAATGG-3'; Reverse: 5'-AACAAAGTCTGGCCTGTATCCAA-3').

For PCR to detect *lpl* delta band after Cre mediated recombination, sequences of primers were set as follows: Forward 5'-CGCCCTGGAACATCACTAAT-3'; Reverse: 5'-CTTCTCAATTGTGGGCAGGT-3'. WT band is of about 2000 bp, delta band is 409 bp.

Western blot

Tissues from MBH of each experimental group were snap frozen. Cells were collected by scraping and sonication with RIPA buffer (R0278, sigma). Protein concentration was determined by BCA assay. The same amount of protein from lysates was placed in 1.5 mL tubes. 4x NuPAGE LDS Sample Buffer (invitrogen, cat.NP0007) was added to each and incubated at 95°C for 5 min. After heating, the mixture was kept on ice for 20 min. 20 ug protein lysates from each sample were then separated by 10% precast gel (Bio-Rad cat.400096180), and transferred to nitrocellulose membranes (Bio-Rad cat.170-4159). After the transfer, the membranes were blocked in 5% milk for 1 hour. Primary antibodies were diluted in 5% milk and incubated with the membrane overnight at 4°C. (Rabbit anti pNF-κB, cell signaling, cat.3033; Rabbit anti-beta-actin, cell signaling, cat.4970); On the following day, membranes were washed by Tris-buffered saline with Tween (TBST) three times for 10 min and incubated with the HRP conjugated secondary antibody for 1 hour at room temperature and washed again in TBST (three times for 10 min). Membranes were then developed by ECL (Bio-Rad, cat.170-5060) and imaged with Odyssey imaging system (LI-COR Bioscience)

Targeted lipidomic analysis

Total lipids of primary microglia (~200 µg protein) were extracted twice according to Folch et al. (Folch et al., 1957) using chloroform/methanol/water (2/1/0.6, v/v/v) containing 500 pmol butylated hydroxytoluene, 1% acetic acid, and 100 pmol of internal standards (ISTD, 17:0-17:0 PC, 19:0-19:0 PC, 17:0-17:0 PE, 17:0-17:0 PS, 17:0-17:0 PG, Avanti Polar Lipids) per sample. Extraction was performed under constant shaking for 60 min at room temperature (RT). After centrifugation at 1,000 x g for 15 min at RT the lower organic phase was collected. 2.5 ml chloroform was added to the remaining aqueous phase and the second extraction was performed as described above. Combined organic phases of the double-extraction were dried under a stream of nitrogen and resolved in 150 µl methanol/2-propanol/water (6/3/1, v/v/v) for UPLC-TQ analysis. Chromatographic separation was modified after Knittelfelder et al. (Knittelfelder et al., 2014) using an AQUITY-UPLC system (Waters Corporation), equipped with a Kinetex C18 column (2.1x50 mm, 1.7 µm; Phenomenex) starting a 15 min gradient with 100% solvent A (MeOH/H₂O, 1/1, v/v; 10 mM ammonium acetate, 0.1% formic acid). A EVOQ Elite™ triple quadrupole mass spectrometer (Bruker) equipped with an ESI source was used for detection. Lipid species were analyzed by selected reaction monitoring (PC: MH⁺ to m/z 184, 25 eV, PE: MH⁺ to -m/z 141, 20 eV, PI: M-H to FA⁻, 50 eV). Data acquisition was done by MS Workstation (Bruker). Data were normalized for recovery and extraction- and ionization efficacy by calculating analyte/ISTD ratios.

Immunohistochemical and immunofluorescent stainings

Immunohistochemistry was carried out as described before (Gao et al., 2014). Briefly, mice used for immunohistochemistry were perfused and fixed by 4% paraformaldehyde in 0.1 M PBS (pH 7.4) at 4°C. After equilibrated for 48 hours with 30% sucrose in TBS, coronal sections (30 µm) were cut on a cryostat and sections were rinsed in 0.1 M TBS. For staining, 3 coronal sections containing the mediobasal hypothalamus (MBH) per mouse were incubated with primary antibodies at 4°C overnight. Sections were rinsed and incubated in biotinylated secondary antibody and avidin-biotin complex (ABC method, Vector Laboratories, Inc., Burlingame, CA). The reaction product was visualized by incubation in 1% diaminobenzidine with 0.01% hydrogen peroxide. For immunofluorescent staining, fluorescent secondary antibodies were added accordingly. Primary antibodies: rabbit anti-iba1 (cat. 234 003, Synaptic Systems), rat anti-CD68 (ab53444, Abcam), rabbit anti-POMC (H-029-30, Phoenix).

Electron microscopy

Brains were perfused and preserved in 4% paraformaldehyde with 0.2% glutaraldehyde. Coronal sections were obtained by a mouse brain slicer matrix. Arcuate nucleus tissue blocks of 1mm³ were dissected and carefully washed in 0.1 M cacodylate washing buffer. Samples were post-fixed in 1% Osmium tetroxide solution and subsequently incubated overnight in 1.5% uranyl acetate solution.

Samples were extensively washed with Milli-Q water and then dehydrated with increasing concentrations of Ethanol (70, 80, 90 and 100%). Then the samples were incubated in Propylene oxide and later embedded in increasing concentrations of epon mix in propylene oxide. Finally, samples embedded in pure epon were placed in blocks for hardening at 60°C. Ultrathin sectioning was conducted using an Ultra Microtome Leica UC6. Several ultra-thin sections of 70 nm were cut and then collected in grids. Grids were contrasted with uranyl acetate and lead citrate prior to imaging. Images were obtained using a FEI Tecnai T12 transmission electron microscope at 100 kV.

Microglia, which could be identified by dense and highly heterochromatin nucleus (Sobaniec-Lotowska, 2005), were imaged at 11000x, 23000x and 68000x magnification for posterior analysis. For each group, at least 20 microglia and adjacent neurons were imaged and quantified. Peri-nuclear mitochondrial ultrastructure in microglia and neurons were analyzed based on following morphological criteria: integrity of inner and outer membranes, cristae structure and electron density of matrix. Autophagosomes in neurons were characterized by double-membrane bound vesicles.

To quantify the Golgi apparatus size, averaged cisternae thickness of each Golgi complex was measured by total Golgi complex width divided by the cisternae number in that Golgi complex. Data were presented as averaged cisternae thickness per cell.

References

- Folch, J., Lees, M., and Sloane Stanley, G.H. (1957). A simple method for the isolation and purification of total lipides from animal tissues. *J Biol Chem* 226, 497-509.
- Garcia-Caceres, C., Quarta, C., Varela, L., Gao, Y., Gruber, T., Legutko, B., Jastroch, M., Johansson, P., Ninkovic, J., Yi, C.X., et al. (2016). Astrocytic Insulin Signaling Couples Brain Glucose Uptake with Nutrient Availability. *Cell* 166, 867-880.
- Knittelfelder, O.L., Weberhofer, B.P., Eichmann, T.O., Kohlwein, S.D., and Rechberger, G.N. (2014). A versatile ultra-high performance LC-MS method for lipid profiling. *J Chromatogr B Analyt Technol Biomed Life Sci* 951-952, 119-128.
- Paxinos, G., and Franklin, K. (2008). *The Mouse Brain in Stereotaxic Coordinates*. Elsevier.
- Sobaniec-Lotowska, M.E. (2005). A transmission electron microscopic study of microglia/macrophages in the hippocampal cortex and neocortex following chronic exposure to valproate. *Int J Exp Pathol* 86, 91-96.